Available online at www.sciencedirect.com
SCIENCE DIRECT®
Catalysis Today 85 (2003) 93–100
CATALYSIS TODAY
www.elsevier.com/locate/cattod

One step towards bridging the materials gap: surface studies of TiO_2 anatase

U. Diebold [a,*], N. Ruzycki [a], G.S. Herman [b], A. Selloni [c]

[a] *Department of Physics, Tulane University, New Orleans, LA 70118, USA*
[b] *Hewlett-Packard Corporation, Corvallis, OR 97330, USA*
[c] *Department of Chemistry, Princeton University, Princeton, NJ 08540, USA*

Abstract

We present a short overview of surface studies on the main low-index surfaces of anatase, the technologically most interesting crystallographic form of titanium dioxide. Results are compared to the extensively investigated surfaces of TiO_2 rutile. The anatase (1 0 1) surface is stable in a (1×1) configuration. It exhibits twofold coordinated (bridging) oxygen atoms and fivefold coordinated Ti atoms with a density comparable to the one found on rutile (1 1 0). Step edges are terminated by fourfold coordinated Ti sites. In contrast to rutile (1 1 0), anatase (1 0 1) does not show a strong tendency for losing twofold coordinated oxygen atoms upon annealing in ultrahigh vacuum. The apparent lack of point defects is also reflected in the adsorption/desorption behavior of water and methanol. The anatase (1 0 0) surface has the second-lowest surface energy and tends to from a (1×2) reconstruction. A model with (1 0 1)-oriented microfacets agrees with the observed features in atomically-resolved STM images. The (0 0 1) surface forms a (1×4) reconstruction that is well explained by an 'ad-molecule' model predicted from density functional theory calculations. A (1×3) reconstruction was observed for the anatase (1 0 3) surface.

Keywords: TiO_2; Surface studies; Photocatalytic reactions; Scanning Tunneling Microscopy; Single crystalline surfaces; Surface reconstruction; Adsorption

1. Introduction

Most commercial titania powder catalysts are a mixture of rutile and anatase, e.g., the most often used Degussa P25 contains approximately 80–90% anatase and the rest rutile [1]. For certain photocatalytic reactions and non-photoinduced catalysis high anatase percent mixtures work best [2]. There is growing evidence that anatase is more active than rutile for O_2 photo-oxidation, but not necessarily for all photocatalytic processes. Anatase behaves differently than rutile in gas-sensing devices, and most photovoltaic cells are based on granular thin films with an anatase structure [3]. Anatase and rutile show inherent particle size differences and this might cause some of the observed differences in chemical properties. However, in order to gain a better understanding of TiO_2-based devices, it is clearly important to obtain atomic-scale information on well-characterized anatase surfaces. So far, surface science investigations for titanium dioxide have mostly focused on rutile, and a quite extensive database on the structural properties, reconstructions, metal overlayer growth, and chemical reactivity of rutile is now available [4]. While the rutile and anatase structure have many similarities they also differ in a variety of ways. In both structures, Ti atoms

* Corresponding author. Tel.: +1-504-862-8279; fax: +1-504-862-3179.
E-mail address: diebold@tulane.edu (U. Diebold).

0920-5861/$ – see front matter © 2003 Elsevier B.V. All rights reserved.
doi:10.1016/S0920-5861(03)00378-X

(formally in a +4 oxidation state) are coordinated to six oxygen atoms (formally O^{2-}), and the O atoms are linked to three Ti atoms. The octahedron of anatase is somewhat more distorted than that of rutile, which has consequences for the crystal-field splitting of the density of states [5]. The mass density of the anatase phase is lower, and the band gap of anatase is somewhat wider, which affects the photocatalytic activity.

Experimental surface science results on anatase are still relatively sparse, and considerations which surface orientations would be relevant are in order. High-purity titania powder catalysts are typically made in a flame process from titanium tetrachloride [1]. Many additional synthetic techniques processes have been applied [6–10]. The shapes of the crystallites vary with preparation techniques and procedures. Typically, (1 0 1) and (1 0 0)/(0 1 0) surface planes are found, together with some (0 0 1) [11]. Several theoretical studies have predicted the stability of the different low-index anatase surfaces [11–15]. The (1 0 1) face is the thermodynamically most stable surface, see the calculated surface energies in Table 1 [14,15]. While it is difficult to obtain accurate values for surface energies with density functional theory (DFT) calculations, the relative surface energies in Table 1 are still meaningful. The calculated Wulff shape of an anatase crystal, based on these numbers, compares well with the shape of naturally-grown mineral samples, see Fig. 1. Interestingly, the average surface energy of an equilibrium-shape anatase crystal is smaller than the one of rutile [14,15], which might explain the fact that nanoscopic TiO_2 particles are more stable in the anatase phase.

Table 1
Comparison of calculated surface formation energies (in J/m^2) for relaxed, unreconstructed TiO_2 surfaces. Two different structures for the (1 0 3) surfaces (a 'faceted' and a 'smooth' one) have been considered; from Refs. [14,15]

Rutile (1 1 0)	0.31
Anatase (1 0 1)	0.44
(1 0 0)	0.53
(0 0 1)	0.90
$(1\,0\,3)_f$	0.83
$(1\,0\,3)_s$	0.93
(1 1 0)	1.09

Experimental investigations on single-crystalline anatase surfaces are just starting [4]. Meaningful surface science investigations necessitate single-crystalline samples. While synthetic rutile crystals are readily available, sufficiently large and pure anatase crystals are more difficult to obtain. Because anatase is a metastable phase, it transforms into rutile. The transition temperature depends on a variety of factors including impurities, crystal size, and sample history. Recently, this problem has been addressed by growing TiO_2 films on $SrTiO_3$ (0 0 1) [16,17] and $LaAlO_3$ [18] but only the (0 0 1) crystallographic surface of anatase can be studied in this manner. Some groups have used

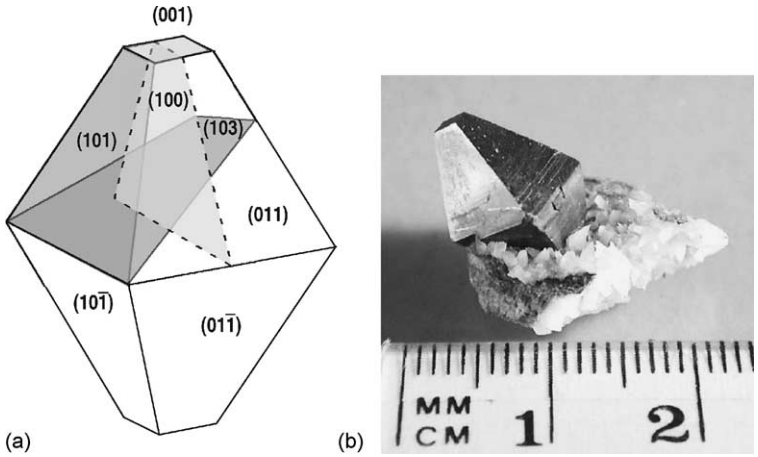

Fig. 1. (a) The equilibrium shape of a TiO_2 crystal in the anatase phase, according to the Wulff construction and surface energies given in Table 1. The crystallographic planes that have been investigated with surface science techniques are indicated. (b) Photograph of an anatase mineral crystal.

synthetically grown anatase [6,19–22], however, these samples are typically small and take a considerable length of time to grow. Alternatively, one can use mineral samples [17,23,24], as large, well ordered, single-crystalline, and relatively pure specimens can be found in nature, see Fig. 1. This approach is the one pursued by our group. While working with minerals poses its own difficulties (some crystals are purer than others; if inclusions are present polishing can lead to rough surfaces; the growth parameters for an epitaxial TiO_2 overlayer that 'covers up' most of the impurities need to be optimized [17]), high-quality STM images and meaningful surface chemistry data have been obtained from such samples.

1.1. Anatase (1 0 1)

A mineral sample similar to the one displayed in Fig. 1 was used in a scanning tunneling microscopy (STM) study of anatase (1 0 1) [22]. In order to avoid the contaminations in this natural single crystal, a 700 Å thick, epitaxial film was grown on the surface, as described in Ref. [17]. Sputtering and annealing produces a (1×1) termination in LEED [20,22], consistent with the low surface energy of the (1 0 1) face. The surface resembles the bulk truncated termination pictured in Fig. 2a. The surface has only pm symmetry, giving rise to a preferential orientation of step edges and triangular terraces (Fig. 3a). A reasonable model for steps edges was derived [22] using the concept of auto-compensation. Titanium atoms at the terraces are fivefold and sixfold coordinated, and titanium atoms at the step edges are fourfold coordinated. These have a higher reactivity against gas adsorption as seen in Fig. 3b [22]. The density of the fivefold coordinated Ti atoms is similar for anatase (1 0 1) and rutile (1 1 0) (5.16×10^{14} and 5.20×10^{14} sites/cm^2, respectively). Twofold coordinated oxygen atoms are located at the ridges of a sawtooth like structure, see Fig. 2a. According to the calculations in Ref. [11], they relax inwards by ∼0.21 Å. The threefold coordinated O atoms relax outwards by 0.06 Å and the fivefold coordinated Ti atoms inwards by ∼0.17 Å, so that the surface exhibits a slightly buckled geometry. The tunneling site in the atomically-resolved STM image in Fig. 3a probably extends across both, the twofold coordinated oxygen atoms and the fivefold coordinated Ti atoms. In images taken with a higher tunneling current (12 nA

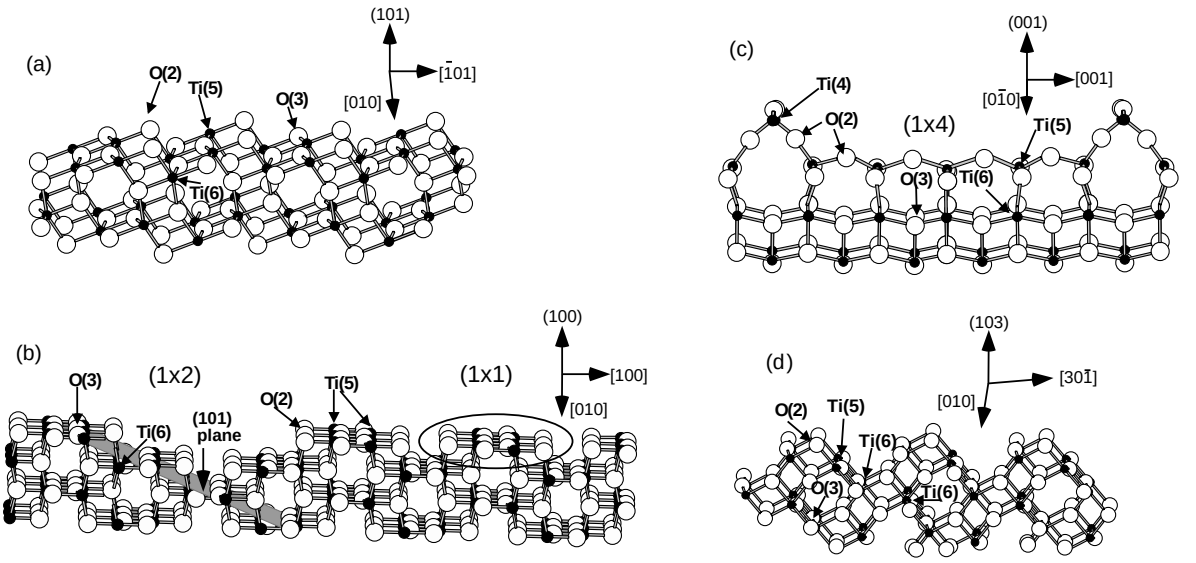

Fig. 2. Atomic models of anatase surfaces: (a) anatase (1 0 1)-(1×1) surface; (b) anatase (1 0 0) surface in a (1×1) configuration (right side) and in a (1×2) configuration (left side) with (1 0 1) microfacets that have been formed by removing the circled region on the right; (c) the ADM model of the anatase (0 0 1)-(1×4) reconstruction proposed by Lazzeri and Selloni [41]; (d) anatase (1 0 3)-(1×1). This surface reconstructs to a $(1 \times n)$ termination.

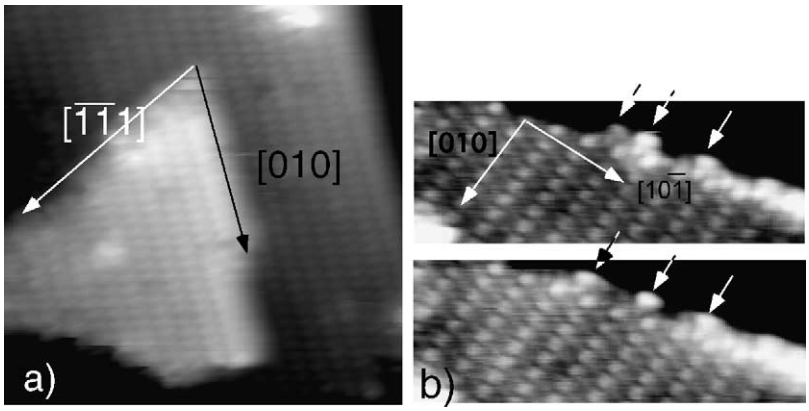

Fig. 3. STM images of anatase (1 0 1): (a) image size 50 Å × 50 Å. The step edges parallel to the [$\bar{1}\bar{1}$1] direction contain fourfold coordinated Ti atoms; (b) image size 73 Å × 23 Å. The image has been taken with an unusually high tunneling current (12 nA). Under these conditions the somewhat brighter atoms probably represent bridging oxygen atoms. Three unidentified adsorbates, marked with arrows, are adsorbed at the step edge, and one of these adsorbates switched sites between taking these images.

in Fig. 3b), where the tip is closer to the surface, the twofold coordinated oxygen atoms are distinguished as independent features.

In correspondence to the rutile (1 1 0) surface, one might expect that the twofold coordinated oxygen atoms are removed easily upon annealing in UHV, and thus give rise to point defects. While several types of imperfections with atomic dimensions are identified in atomically-resolved images, they do not exhibit the unique signature of point defects that is typically observed on rutile (1 1 0) [25,26], or the hydroxylated point defects described in Ref. [27]. In addition their number density is very small, certainly less than the usually quoted 5–10% on rutile (1 1 0) [28,29]. This would be in agreement with the (calculated) low surface energy of the (1 0 1) surface [11,14,15]. Calculations of the electrostatic potential by Woning and Santen [30] also predict that it is easier to reduce the rutile (1 1 0) surface than the anatase (1 0 1) surface. Note that the twofold coordinated O anions at the edges of the sawtooth profile in Fig. 2 are bound to the fivefold coordinated Ti cations, while the rutile surface is flat with twofold coordinated bridging oxygens bound to sixfold coordinated Ti cations and projected out of the surface plane. Removal of one twofold coordinated bridging oxygen results in two fourfold coordinated Ti^{3+} cations and two fivefold coordinated Ti^{3+} cations for the anatase and rutile surface, respectively. These highly under-coordinated Ti cations for anatase are likely to be less stable than the Ti cations for rutile, and may explain why the number of oxygen vacancies at the surface of anatase (1 0 1) is much lower than the one observed for rutile (1 1 0).

The structural similarity between the non-defective rutile (1 1 0) and the anatase (1 0 1) surface is reflected in the adsorption and desorption behavior of two simple test molecules, water and methanol [31]. Both adsorbates have been studied extensively on rutile (1 1 0) [4,29,32,33], and their adsorption behavior on this surface is well understood. The adsorption of water and methanol on the anatase (1 0 1) surface was investigated with thermally programmed desorption (TPD) and X-ray photoelectron spectroscopy (XPS) [31]. XPS showed that adsorbed water and methanol are predominately adsorbed to the surface in a molecular state without dissociating. TPD shows three peaks, desorption of multilayer water (at 160 K), desorption of water bound to twofold coordinated oxygen (at 190 K), and water adsorbed at fivefold coordinated titanium, desorbing from the surface around 250 K. This assignment was partially based on the similarity of these TPD peaks with results from rutile (1 1 0) [33]. The saturation coverage of the chemisorbed water correlates well with the density of fivefold coordinated Ti atoms on the anatase (1 0 1) surface. Overall, these experimental results match well the adsorption geometry predicted by DFT calculations [11], where water was found to bind preferentially to Ti(5) atoms with

the H atoms directed towards the neighboring bridging oxygen atoms. Water also adsorbs molecularly on rutile (1 1 0), except at the point defects, where recombinative desorption is observed at ∼500 K. Such a defect-related dissociation of water is absent on the anatase (1 0 1) surface, in agreement with the apparent lack of point defects in STM images.

TPD spectra of methanol on anatase (1 0 1) showed desorption around 135, 170, 260, 410 and 610 K. The first two peaks were related to multilayers of methanol and methanol adsorption to the twofold coordinated oxygen, respectively [31]. Molecular methanol, adsorbed to the fivefold coordinated Ti atoms, leaves the surface around 260 K, and the peak at 410 K is assigned to methoxy adsorbed to the fivefold coordinated titanium. A small TPD feature at 610 K is probably linked to methoxy adsorbed at the Ti step edges. Overall the methanol TPD spectra from anatase (1 0 1) resemble those from oxidized rutile (1 1 0), but no evidence was found for oxidation of methanol to formaldehyde on the anatase surface.

1.2. Anatase (1 0 0)

According to the low surface energy in Table 1, the anatase (1 0 0) surface should be quite stable. While a Wulff construction results in an equilibrium-shape crystal without a terminating (1 0 0) plane (Fig. 1), such surfaces are observed in powder materials. Structural investigations were performed on a sample that was cut from a natural mineral crystal. Low-energy electron diffraction (LEED) of a sputtered/annealed surface indicates a $(1 \times n)$ reconstruction [34]. STM shows that the (1 0 0) surface is characterized by bright ridges running in the [0 1 0] direction (Fig. 4). The distance between two of these ridges is approximately 18 Å, consistent with a (1×2) periodicity.

The STM results seem qualitatively consistent with the (1 0 1)-microfaceted model shown in Fig. 2b. On the right side of the model is the (1×1) terminated surface. The (1 0 0) surface consists of fivefold coordinated Ti atoms and twofold coordinated O atoms, with threefold coordinated O and sixfold coordinated Ti as in the bulk. Reconstruction occurs when the encircled top unit is removed in Fig. 2b, resulting in a surface with (1 0 1) microfaceted grooves running in the [0 1 0] direction. This creates similar local environments on the reconstructed anatase (1 0 0) and the flat anatase (1 0 1)-(1×1) surfaces. Without first-principles total-energy calculation one can only speculate what the driving force of this reconstruction might be. On the one hand, the (1 0 1) planes on the microfacets have a lower energy. On the other hand, the total surface area is increased by the faceting. In a simple estimate these two effects cancel each other. The separation between the under-coordinated Ti atoms is increased in the microfaceted model, however, which may explain the reconstruction dynamics.

Ridge arrangement is not completely uniform on the surface, with an occasional bright ridge growing

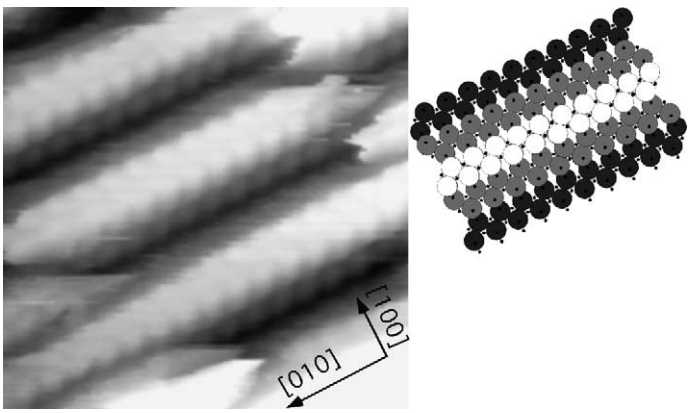

Fig. 4. STM image (50 Å × 50 Å, $V_{sample} = +2.0$ V, $I_{tunnel} = 6.0$ nA) of the reconstructed anatase (1 0 0) surface. The separation between the bright ridges is ∼18 Å indicating a (1×2) termination. The atomic model (large balls: Ti atoms, small dots: O atoms) of the (1 0 1) microfaceted model for the (1×2) reconstruction, also presented in Fig. 2b, agrees well with the STM image.

in between two lower lying ridges, see Fig. 4. This is due to the top unit (circled in Fig. 2b) not being completely removed, which causes a bright row to appear. The arrangements are more irregular on a larger scale, giving rise to the observed $(1 \times n)$ periodicity in LEED. In Fig. 4, the microfaceted model of the surface is shown alongside the STM image. The model shows a good correspondence to the image. Similar to anatase (1 0 1) STM does not show any additional bright spots or 'missing' atoms that could be assigned to point defects. Again, this might be due to the difficulty in separating the twofold coordinated O atoms from the fivefold coordinated Ti atoms in STM, or the fact that this surface does not reduce easily. Because a microfaceted surface has essentially the same geometry as a (1 0 1) surface, the surface chemistry of these two orientations might be quite similar.

1.3. Anatase (0 0 1)

The stable, auto-compensated anatase (0 0 1) surface exhibits exclusively fivefold coordinated Ti atoms, as well as twofold and threefold coordinated oxygen atoms [14,15] (see the center part of Fig. 2c). Calculations show that the corrugation increases somewhat upon relaxation, from 0.82 to 0.92 Å [11].

The most detailed structural investigations on this surface so far have been performed on thin films, grown epitaxially on the $SrTiO_3$ (0 0 1) substrates [16,17,35]. The $SrTiO_3$ (0 0 1) surface shows a poor lattice match with the rutile phase but an excellent match with the anatase (0 0 1) surface (−3%). The anionic sublattices of substrate and film bear substantial resemblance despite their overall crystallographic dissimilarities [36]. Heteroepitaxial growth of TiO_2 can be regarded as a continuous formation and extension of the oxygen atom network from the $SrTiO_3$ substrate into the anatase film. Within this oxygen sublattice the (relatively small) Ti cations arrange in their appropriate sites. Formation of interfaces where the oxygen sublattice continues and the metal cation sublattice changes abruptly is often exploited for thin film heteroepitaxy of metal oxides [37]. On $SrTiO_3$ (0 0 1) epitaxial, stoichiometric anatase thin films of high crystalline quality have been grown by several techniques [17,36,38] and do not transform into rutile at annealing temperatures up to 1000 °C [17].

The (0 0 1)-(1×1) surface is not very stable, however, and reconstructs when heated to elevated temperatures [19,35,39,40]. Only on as-grown samples that were slightly contaminated with carbon a (1×1) terminated surface was observed [16]. Herman et al. [35] were the first to point out that a two-domain (1×4) reconstruction formed on an anatase film on $SrTiO_3$ after sputtering and annealing the (1×1) surface in UHV. Based on angle resolved mass spectroscopy of recoiled ions (AR-MRSI) a 'microfaceted' model was proposed. In this model (1 0 3) facets are exposed which contain twofold oxygen and both fourfold and fivefold coordinated Ti atoms. The appearance of the (1×4) reconstruction in STM is not consistent with the (1 0 3) microfaceted model [39]. Based on first-principles calculations, Lazzeri and Selloni [41] suggested the so-called 'added molecule' (ADM) structure, see Fig. 2c. High-resolution STM and NC-AFM images are consistent with the ADM model [40]. Tanner et al. [40] reported adsorption of carboxylic acids on the (1×4) reconstructed anatase (0 0 1) surface. At high coverages, a (2×4) overlayer of dissociated carboxylates was observed. Single carboxylate bind to the positions centered atop the (1×4) rows, consistent with fourfold coordinated Ti atoms on top of the ADM structure in Fig. 2c.

1.4. Anatase (1 0 3)

Two (1×1) surface terminations of a (1 0 3) plane were considered in the DFT calculations by Lazzeri et al. [14,15], see Table 1. The one called 'faceted' exhibits a somewhat smaller surface formation energy and is depicted in the model in Fig. 2d. On the 'faceted' (1 0 3) surface (0 0 1) and (1 0 0) microfacets run along the $[3\,0\,\bar{1}]$ direction in a sawtooth pattern. Given the fact that neither of these planes is stable in a (1×1) configuration it is not too surprising that the anatase (1 0 3) surface was found experimentally to reconstruct as well.

A natural mineral crystal was cut in (1 0 3) direction and investigated with LEED and STM. This sample was considerably more contaminated than other specimen, however, and a persistent Ca impurity could not be removed completely in sputtering/annealing cycles. LEED exhibited sharp (1×1) spots, with diffuse lines in one direction, see Fig. 5a, suggesting a reconstruction with $(1 \times n)$ periodicity. The STM

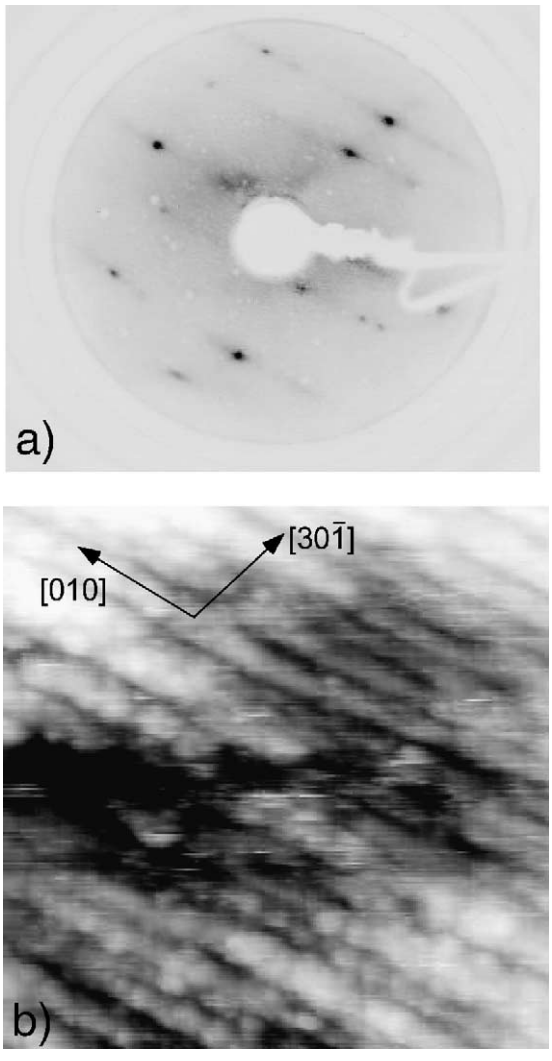

Fig. 5. (a) LEED of a reconstructed anatase (1 0 3)-(1 × *n*) surface; (b) STM image (500 Å × 500 Å, V_{sample} = +2.2 V, I_{tunnel} = 2.9 nA). Row separations are multiples of the unit cell distance in [3 0 $\bar{1}$] direction (14.8 Å^2).

results in Fig. 5b are consistent with a (1 × *n*) reconstruction. The rows are fairly parallel, with the distance between the rows being two, three and even four times the lattice constant in [3 0 $\bar{1}$] direction (14.8 Å). The (1 × 3) periodicity was noted to occur more frequently than the other spacings. The surface termination may be affected by the presence of impurities, as the LEED patterns and STM images varied with the concentration of calcium as measured with low-energy He^+ ion scattering (LEIS).

Although interpretation of the results on the (1 0 3) surface are complicated by the these impurities, a model similar to the (1 0 0)-(1 × 2) surface (Fig. 2b) could be invoked to explain the (1 × 3) reconstruction. It would result in [0 1 0] oriented grooves that consist of (1 0 1) and (0 0 1)-type surfaces on the side. However, the depth of such grooves would be greater than what is observed with STM. Additionally, the unreconstructed (0 0 1) surface has a high surface energy, which would suggest additional reconstructions on at least one side of the grooves. Calculations and better-resolved STM images are necessary to further reveal the exact nature of the reconstructed anatase (1 0 3) surface.

2. Summary

The geometry of all the relevant low-index surfaces of TiO_2 anatase has now been characterized, and preliminary surface chemistry experiments have been performed. The anatase (1 0 1) surface is the only orientation that does not reconstruct and, except for some relaxations, exhibits a bulk-terminated configuration. The density as well as the nature of undercoordinated surface atoms on anatase is quite similar to what is found on the rutile (1 1 0) surface; one main difference between the two systems is an apparent lack of point defects on anatase (1 0 1). The similarity of these two systems suggests that the rich knowledge, obtained from years of surface studies on rutile (1 1 0), can be used for a predictive understanding of surface chemistry on the molecular scale on anatase (1 0 1). This is supported by experimental adsorption/desorption results of water and methanol on anatase (1 0 1); however, a more extensive data set is needed to firmly draw such a conclusion.

The anatase (1 0 0) surface reconstructs to possibly form (1 0 1) oriented microfacets under typical preparation conditions in UHV. It is thus suggested that the surface chemistry of this plane would largely resemble that of the (1 0 1) surface, this conjecture is awaiting experimental confirmation. The anatase (0 0 1) surface also reconstructs, and the available STM, non-contact AFM, and adsorption data are compatible with the theoretically-suggested 'ADM' model. The undercoordinated Ti atoms on top of the added units are highly reactive. The (1 0 3) surface shows a

reconstruction resulting in ridges running along the [0 1 0] direction.

With these surface characterization results and preliminary adsorption studies of simple test molecules, the groundwork is laid for more extensive surface chemistry experiments that should pinpoint the reasons for the different (photo)catalytic reactivity of the rutile and anatase surfaces.

Acknowledgements

This work was supported by DoE grant DE-FG02-00ER45834 and NSF grant CHE-0109804.

References

[1] C.N. Satterfield, Heterogeneous Catalysis in Industrial Practice, 2nd ed., McGraw-Hill, New York, 1991.
[2] T. Ohno, K. Sarukawa, M. Matsumura, J. Phys. Chem. B 105 (2001) 2417.
[3] B. O'Regan, M. Grätzel, Nature 353 (1991) 737.
[4] U. Diebold, Surf. Sci. Rep. 48 (2003) 53.
[5] N. Ruzycki, G.P. Zhang, T. Schuler, T.A. Calcott, U. Diebold, D.L. Ederer, in preparation.
[6] L. Kavan, M. Grätzel, S.E. Gilbert, C. Klemenz, H.J. Scheel, J. Am. Chem. Soc. 118 (1996) 6716.
[7] J.M.G. Amores, V.S. Escribano, G. Busca, J. Mater. Chem. 5 (1995) 1245.
[8] C. Byun, J.W. Jang, I.T. Kim, K.S. Hong, B.-W. Lee, Mater. Res. Bull. 32 (1997) 431.
[9] P. Arnal, R.J.P. Corriu, D. Leclercq, P.H. Mutin, A. Vioux, J. Mater. Chem. 6 (1996) 1925.
[10] T. Oyama, Y. Iimura, K. Takeuchi, T. Ishii, J. Mater. Sci. Lett. 15 (1996) 594.
[11] A. Vittadini, A. Selloni, F.P. Rotzinger, M. Grätzel, Phys. Rev. Lett. 81 (1998) 2954.
[12] A. Fahmi, C. Minot, Surf. Sci. 304 (1994) 343.
[13] T. Bredow, K. Jug, Surf. Sci. 327 (1995) 398.
[14] M. Lazzeri, A. Vittadini, A. Selloni, Phys. Rev. B 63 (2001) 155409/1.
[15] M. Lazzeri, A. Vittadini, A. Selloni, Phys. Rev. B 65 (2002) 119901/1.
[16] G.S. Herman, Y. Gao, T.T. Tran, J. Osterwalder, Surf. Sci. 447 (1999) 201.
[17] G.S. Herman, Y. Gao, Thin Solid Films 397 (2001) 157.
[18] S.A. Chambers, C.M. Wang, S. Thevuthasan, T. Droubay, D.E. McCready, A.S. Lea, Thin Solid Films 418 (2002) 197.
[19] R. Hengerer, L. Kavan, M. Grätzel, J. Electrochem. Soc. 147 (2000) 1467.
[20] R. Hengerer, B. Bolliger, M. Erbudak, M. Grätzel, Surf. Sci. 460 (2000) 162.
[21] R. Hengerer, L. Kavan, B. Bolliger, M. Erbudak, M. Grätzel, Mater. Res. Soc. Symp. Proc. 623 (2000) 43.
[22] W. Hebenstreit, N. Ruzycki, G.S. Herman, Y. Gao, U. Diebold, Phys. Rev. B 64 (2000) R16344.
[23] G. Silversmit, H. Poelman, L. Fiermans, R. De Gryse, Solid State Commun. 119 (2001) 101.
[24] H. Poelman, L. Fiermans, Surf. Sci. Spectra 5 (1998) 252.
[25] U. Diebold, J. Lehman, T. Mahmoud, M. Kuhn, W. Hebenstreit, G. Leonardelli, M. Schmid, P. Varga, Surf. Sci. 411 (1998) 137.
[26] U. Diebold, J.F. Anderson, K.O. Ng, D. Vanderbilt, Phys. Rev. Lett. 77 (1996) 1322.
[27] R. Schaub, P. Thostrup, N. Lopez, E. Laegsgaard, I. Stensgaard, J.K. Norskov, F. Besenbacher, Phys. Rev. Lett. 87 (2001) 266104/1.
[28] U. Diebold, J. Lehman, T. Mahmoud, M. Kuhn, G. Leonardelli, W. Hebenstreit, M. Schmid, P. Varga, Surf. Sci. 411 (1998) 137.
[29] M.A. Henderson, Surf. Sci. 355 (1996) 151.
[30] J. Woning, R.A.V. Santen, Chem. Phys. Lett. 101 (1983) 541.
[31] G.S. Herman, Z. Dohnalek, N. Ruzycki, U. Diebold, J. Phys. Chem. B 107 (2003) 2788.
[32] M.A. Henderson, S. Otero-Tapia, M.E. Castro, Faraday Discuss. Chem. Soc. 114 (1999) 313.
[33] M.A. Henderson, Langmuir 12 (1996) 5093.
[34] N. Ruzycki, G. Herman, L.A. Boatner, U. Diebold, Surf. Sci. 529 (2003) L239.
[35] G.S. Herman, M.R. Sievers, Y. Gao, Phys. Rev. Lett. 84 (2000) 3354.
[36] S. Chen, M.G. Mason, H.J. Gysling, G.R. Paz-Pajult, T.N. Blanton, K.M. Chen, C.P. Fictorie, W.L. Gladfelter, A. Franciosi, P.I. Cohen, J.F. Evans, J. Vac. Sci. Technol. A 11 (1993) 2419.
[37] S.A. Chambers, Surf. Sci. Rep. 39 (2000) 105.
[38] W. Sugimura, A. Yamazaki, H. Shigetani, J. Tanaka, T. Mitsuhashi, Jpn. J. Appl. Phys. 36 (1997) 7358.
[39] Y. Liang, S. Gan, S.A. Chambers, E.I. Altman, Phys. Rev. B 63 (2001) 235402/1.
[40] R.E. Tanner, A. Sasahara, Y. Liang, E.I. Altman, H. Onishi, J. Phys. Chem. B 106 (2002) 8211.
[41] M. Lazzeri, A. Selloni, Phys. Rev. Lett. 87 (2001) 266105/1.